Separation Science and Technology
Publication details, including instructions for authors and subscription information:
http://www.informaworld.com/smpp/title~content=t713708471

Combination of Sorption-Enhanced Steam Methane Reforming and Electricity Generation by MCFC: Concept and Numerical Simulation Analysis

Wei Yan[a]; Sheng Sui[a]; Guohua Xiu[b]; Yanfang He[a]
[a] Institute of Fuel Cell, Shanghai Jiao Tong University, Shanghai, China [b] Linde Technology Center, Shanghai, China

To cite this Article Yan, Wei , Sui, Sheng , Xiu, Guohua and He, Yanfang(2009) 'Combination of Sorption-Enhanced Steam Methane Reforming and Electricity Generation by MCFC: Concept and Numerical Simulation Analysis', Separation Science and Technology, 44: 13, 3013 — 3044
To link to this Article: DOI: 10.1080/01496390903182560
URL: http://dx.doi.org/10.1080/01496390903182560

Separation Science and Technology, 44: 3013–3044, 2009

ISSN: 0149-6395 print/1520-5754 online
DOI: 10.1080/01496390903182560

Taylor & Francis
Taylor & Francis Group

Combination of Sorption-Enhanced Steam Methane Reforming and Electricity Generation by MCFC: Concept and Numerical Simulation Analysis

Wei Yan,[1] Sheng Sui,[1] Guohua Xiu,[2] and Yanfang He[1]
[1]Institute of Fuel Cell, Shanghai Jiao Tong University, Shanghai, China
[2]Linde Technology Center, Shanghai, China

Abstract: Reformed gas made by the steam methane reforming(SMR) process is used as fuel feed to MCFC, but it is not as good as pure hydrogen due to the presence of CO_2 and CO. The sorption-enhanced steam methane reforming (SE-SMR) process can reduce CO_2 and CO to a low level and produce high purity hydrogen. Considering the merits of similar operating temperatures (about 500°C) and carbon dioxide recycle, a novel concept of a six-step sorption-enhanced steam methane reforming (SE-SMR) combined with electricity generation by molten carbonate fuel cell (MCFC) is proposed. In the present paper, a cycle of the SE-SMR process, which include the steps of reaction/adsorption, depressurization, gas purges (nitrogen and reformed gas, respectively), and pressurization with reformed gas, is modeled and analyzed. The process stream in the SE-SMR process is used as anode feed in MCFC. According to the result of numerical simulation, a fuel cell grade hydrogen product (above 80% purity) at the SE-SMR temperature of 450°C can be obtained. A carbon dioxide recycle mechanism is developed for cathode feed of MCFC from flue gas by burning with excess air to achieve a proper CO_2/air ratio (about 30:70). The novel electricity generation system, which can operate at lower energy consumption and high purity hydrogen feed is helpful for the MCFC'S performance and life time.

Keywords: Carbon dioxide recycle, electricity generation system, molten carbonate fuel cell (MCFC), numerical simulation, regeneration, sorbent, Sorption-enhanced Steam Methane Reforming (SE-SMR)

Received 26 September 2008; accepted 12 May 2009.

Address correspondence to Sheng Sui, Institute of Fuel Cell, Shanghai Jiao Tong University, Shanghai 200240, China. Fax: +86-21-34206249. E-mail: ssui@sjtu.edu.cn

INTRODUCTION

To respond to the sharp growth of energy consumption and environmental pollution concerns in the modern economy, the development of electricity generation systems with readily available fuels, high efficiency, and minimal environmental impact are required. Fuel cell technology is being increasingly considered as one of the promising solutions. Fuel cell-based power plants convert the chemical energy of fuels directly to electricity without the conversion of chemical energy into heat. It has the advantages of high efficiency and low pollutant emissions in comparison to traditional fossil fuel-based energy conversion devices. Among the various fuel cell types, molten carbonate fuel cell (MCFC) is a potential technology and now commercially available (1).

By far the most efficient way to apply MCFC for power generation is by performing the steam-reforming reaction within the MCFC stack, the so-called internal reforming (IR). In this way, the synergy is maximal because the reaction products from the steam-reforming reaction are used for the cell reaction $2H_2 + O_2 = 2H_2O$, while the heat required for steam-methane reforming is provided by the cell reaction (2,3). Also, the Tomczyk group (3) and the German company MTU are working on the IR MCFC systems which have an electrical efficiency of about 45% and a thermal efficiency of 32%. The main disadvantage of the IR system is that it proves to be too difficult and the volatilization of molten salt is an especially serious subject which deactivates the reforming catalyst.

MCFC normally operates at approximately 650°C. This operating temperature is needed to keep carbonate salt electrolyte in a liquid state and has sufficient ionic conductivity. The high temperature is also advantageous for the system in terms of fast kinetics, non-noble metal catalyst, high quality waste heat, and fuel flexibility (2,3). The conventional MCFC generation systems use natural gas as raw material; before being supplied to the MCFC, natural gas is preceded mainly by the steam methane reforming (SMR) process, which includes a series of stages of the fuel reforming and purification. The energy utilization of the SMR process is not reasonable as the temperature of the process gas has to be raised up, cooled down, and finally raised up again. Also, impurity in the reformed gas from the SMR process is not good for the MCFC system. For example, carbon monoxide in the reformed gas gives excess heat by a water-gas shift (WGS) reaction, which may result in un-uniform temperature distribution on MCFC electrodes and reduce its life time. In addition, about 20% carbon dioxide in the reformed gas dilutes the hydrogen concentration and a suitable amount of steam has to be added to limit the reverse WGS reaction. Thus, if CO and CO_2 in the reformed gas could be greatly reduced or even removed, the performance and life

time of MCFC may be improved. To this aim, a combination system with the SMR process enhanced by sorption reaction and MCFC has been developed.

The advantages of the sorption-enhanced reaction process (SERP) have been widely reported in many literatures (4–10). Many reactions are limited by equilibrium, and the production of hydrogen by steam-methane reforming is a good example. The SERP, involving the addition of sorbent into the reactor bed for selectively uptaking one of the products, makes the equilibrium shifting forward according to the Le Chatelier principle (4–7). The Sircar group (8) proposed that the SERP for SMR uses a fixed-bed reactor packed with a mixture of a nickel catalyst and chemisorbent for the selective removal of CO_2 (one of the reaction products) from the reaction zone. By the SERP, >90 mol.% hydrogen is produced, and impurities in the hydrogen product consist primarily of methane (<10 mol.%) and trace quantities (<50 ppm level) of carbon oxides. The chemisorbent is periodically regenerated by using the principles of pressure swing adsorption (PSA). The reforming reactions in the SERP can be carried out at a moderate temperature range of 450–550°C, which is much less than that in a conventional SMR reactor (700–900°C) packed with a reforming catalyst only. In addition, the Rodrigues group (9) mathematically modeled and analyzed a five-step, one-bed, sorption-enhanced reaction process for hydrogen production by steam methane reforming. The sorbent is also regenerated by PSA. The results showed that the process had a sufficiently high purity of hydrogen (average purity over 80%) with traces of CO and CO_2, high methane conversion, fast adsorbent regeneration, and cyclic steady-state operation.

In recent years, a new concept combining SE-SMR technology with fuel cells has been proposed. Iordanidisa et al. (11). investigated a concept of sorption-enhanced steam reforming of bio-oil/biogas for electricity and heat generation by phosphoric acid fuel cells. The sorptive removal of the CO_2 from the reaction site results in low CO and CO_2 concentrations (<1%) in the reformed gas. The system exhibits 4.6% higher generation efficiency compared to a normal system using bio-oil as a fuel. Lysikova et al. (12). experimentally studied the single-step sorption-enhanced reforming of methane, the propane–butane mixture, ethanol, and methanol over an admixture of CaO sorbent with a Ni reforming catalyst in a periodically operated quasi-adiabatic fixed bed reactor. In the case of the alcohols reforming the hydrogen purity was 98–99% with both CO and CO_2 impurities of about 10–20 ppm. A proton exchange membrane fuel cell (PEMFC) stack was successfully fed with the hydrogen produced by the single-step sorption enhanced reforming of ethanol.

Until now, reports in literatures are limited on that gas for purging in the SE-SMR process is usually inert gas (nitrogen or steam) and the SE-SMR process in an integrated system only provides a hydrogen product for fuel cells.

Due to the operating temperature suitability and carbon dioxide recycle, the combination of SE-SMR and MCFC is an ideal coupling process when compared witht the IR-MCFC system. First, the combined system of SE-SMR and MCFC is not as difficult as the IR-MCFC system. Second, the similar operating temperature of SE-SMR and MCFC means that the reformed gas produced can be directly introduced into MCFC's anode as fuel. Finally, a high hydrogen content is helpful for MCFC's efficiency and life time.

In the present paper, a six-step SE-SMR process for MCFC is proposed as following:

(i) high-pressure reaction/adsorption;
(ii) depressurization;
(iii) the 1st nitrogen purge at low-pressure to remove hydrogen;
(iv) the 2nd nitrogen purge at low-pressure to regenerate the adsorbent;
(v) the reformed gas purge at low-pressure;
(vi) pressurization with the reformed gas.

The parameters of the above process were analyzed for hydrogen production based on process simulation. Furthermore, the compositions of anode feed and cathode feed for MCFC are evaluated, and a new CO_2 recycle mechanism is proposed.

PROCESS DESCRIPTION

The novel integrated electricity generation system of SE-SMR and MCFC fed with natural gas is shown in Fig. 1. The generation system is divided into three function parts:

(i) sorption-enhanced steam methane reforming;
(ii) molten carbonate fuel cell;
(iii) carbon dioxide and flue gas recycle.

The six-step one-bed sorption-enhanced reaction process is shown in Fig. 2. It includes two stages of high-pressure reaction/adsorption and low-pressure adsorbent regeneration (CO_2 desorption).

In the high-pressure reaction/adsorption stage, steam and methane are introduced into the reforming reactor at the H_2O/CH_4 ratio (W/C) 6:1. The reforming reactor mentioned above contains a carbon dioxide

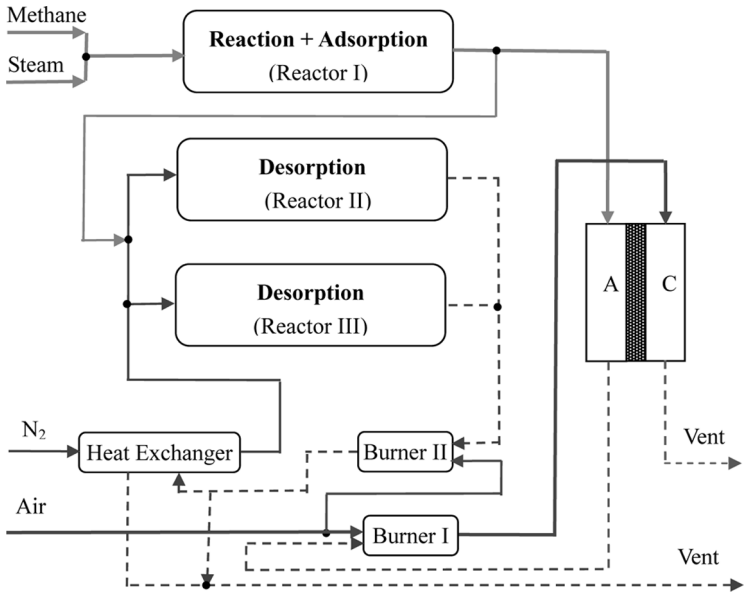

Figure 1. Schematic diagram of novel natural gas MCFC power generation system.

adsorbent and an Ni catalyst. At W/C 6:1, the reaction temperature is 450°C and the pressure is 446 kPa, methane and water are reformed in the reactor and hydrogen is obtained. The reformed gas is supplied to the anode of MCFC. When the average H_2 purity at the reactor outlet ($L = 2$ m) is less than about 80%, the high-pressure reaction/adsorption step is ended and then switched to the CO_2 desorption stage for the adsorbent regeneration.

Adsorbent regeneration (CO_2 desorption) stage mainly consists of five steps:

(i) Depressurization: Pressure in the reforming reactor is reduced to 126 kPa, and the releasing gas (the reformed gas and the desorbed CO_2) is recycled as burner fuel.
(ii) The 1st nitrogen purge: The purpose of this step is to remove hydrogen in the void space of the bed. Nitrogen (>126 kPa) is introduced to lower the hydrogen content to less than 0.5% in the effluent. The combustible compositions in the purged nitrogen are also burned to recover its energy for heating cool nitrogen.
(iii) The 2nd nitrogen purge: Nitrogen as the main purge gas is used to regenerate the adsorbent. The nitrogen purge is ended when the

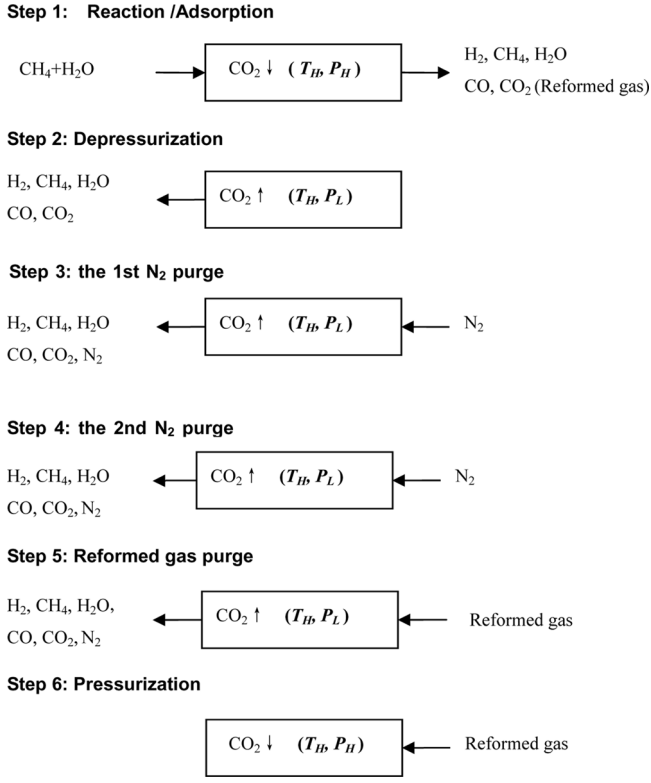

Figure 2. Process steps for the one-bed sorption-enhanced reaction.

CO_2 content in the effluent stream is less than 3.5%. The purged nitrogen with the desorbed CO_2 is vented into the atmosphere.

(iv) The reformed gas purge: The reformed gas is introduced into the reactor to reduce the inert nitrogen content in the hydrogen product, and the effluent is recycled as fuel.

(v) Pressurization with the reformed gas: The pressure of the reactor is increased to 446 kPa for the high-pressure reaction/adsorption step.

To produce the reformed gas and cathode feed continuously for the MCFC, at least two reactors (PSA reactors) are needed to swing between the reaction/adsorption and adsorbent regeneration. In a two-reactor configuration, when one PSA reactor is in the stage of reaction-adsorption, another PSA reactor is in the stage of adsorbent regeneration. Each SE-SMR reforming reactor alternately works between the high-pressure reaction/adsorption stage and the carbon dioxide desorption stage.

In MCFC, the fuel cell grade hydrogen produced in the stage of reaction-adsorption is supplied to the anode; as oxidant, the flue gas of the burnt anode stream with a proper CO_2/air ratio (about 30:70) from the burner is introduced into the cathode.

The electrochemistry reactions in MCFC are described as below:

$$\text{Anode} \quad H_2 + CO_3^{2-} - 2e^- = H_2O + CO_2 \tag{1}$$

$$\text{Cathode} \quad \frac{1}{2}O_2 + CO_2 + 2e^- = CO_3^{2-} \tag{2}$$

The tailed gas from the anode mainly containing excess hydrogen and CO_2 is introduced into the burner for energy and CO_2 recovery. In the burner I, a proper CO_2/air ratio (about 30:70) in the flue gas is kept to meet the requirement of the cathode feed. Then, the flue gas is recycled into the cathode input.

The three main chemical reactions in the SE-SMR process are given as:

$$CH_4 + H_2O \leftrightarrow CO + 3H_2, \ \Delta H_{298} = 206\,\text{kJ/mol} \tag{3}$$

$$CH_4 + 2H_2O \leftrightarrow CO_2 + 4H_2, \ \Delta H_{298} = 164.9\,\text{kJ/mol} \tag{4}$$

$$CO + H_2O \leftrightarrow CO_2 + H_2, \ \Delta H_{298} = -41.1\,\text{kJ/mol} \tag{5}$$

Their reaction kinetic model suggested by Xu and Froment (13) is summarized as:

$$R_1 = \frac{k_1}{P_{H_2}^{2.5}}\left(P_{CH_4}P_{H_2O} - \frac{P_{H_2}^3 P_{CO}}{K_1}\right)/(DEN)^2 \tag{6}$$

$$R_2 = \frac{k_2}{P_{H_2}^{3.5}}\left(P_{CH_4}P_{H_2O}^2 - \frac{P_{H_2}^4 P_{CO_2}}{K_2}\right)/(DEN)^2 \tag{7}$$

$$R_3 = \frac{k_3}{P_{H_2}}\left(P_{CO}P_{H_2O} - \frac{P_{H_2}P_{CO_2}}{K_3}\right)/(DEN)^2 \tag{8}$$

where

$$DEN = 1 + K_{CO}P_{CO} + K_{H_2}P_{H_2} + K_{CH_4}P_{CH_4} + \frac{K_{H_2O}P_{H_2O}}{P_{H_2}} \tag{9}$$

in which $P_i = y_i P$ ($i = CH_4$, H_2O, H_2, CO_2 and CO, P is the local total pressure, y_i is the gas-phase mole fraction of component i). For the expressions of k_1, k_2, and k_3, K_{CH_4}, K_{H_2}, and K_{CO}, K_{H_2O} K_1, K_3, and K_3, see Table 1.

r_i, the formation rate of component i, was calculated by Eqs. (3–5) as the following:

$$r_i = \sum_{j=1}^{3} \upsilon_{ji} R_j \tag{10}$$

where v_{ji} is the stoichiometric coefficient of component i in reaction j. Thus,

$$r_{CH_4} = -R_1 - R_2 \tag{11}$$

$$r_{H_2O} = -R_1 - 2R_2 - R_3 \tag{12}$$

$$r_{H_2} = 3R_1 + 4R_2 + R_3 \tag{13}$$

$$r_{CO} = R_1 - R_3 \tag{14}$$

$$r_{CO_2} = R_2 + R_3 \tag{15}$$

Reforming reactions (Eqs. (3,4)) are strongly endothermic, while the water-gas shift reaction (Eqs. (5)) is moderately exothermic. The reforming

Table 1. Parameters for reaction kinetics, reaction equilibrium and adsorption kinetics (13)

$$k_1 = 1.626 \times 10^{-4} \exp\left[-\frac{240100}{R}\left(\frac{1}{T} - \frac{1}{648}\right)\right] kmol\, bar^{0.5}/kg(cat)h$$

$$k_2 = 2.541 \times 10^{-5} \exp\left[-\frac{243900}{R}\left(\frac{1}{T} - \frac{1}{648}\right)\right] kmol\, bar^{0.5}/kg(cat)h$$

$$k_3 = 7.333 \exp\left[-\frac{67130}{R}\left(\frac{1}{T} - \frac{1}{648}\right)\right] kmol/kg(cat)h\, bar$$

$$K_1 = \frac{1}{\exp(0.2513Z^4 - 0.3665Z^3 - 0.58101Z^2 + 27.1337Z - 3.2770)} atm^2$$

$$K_2 = K_1 K_3$$

$$K_3 = \exp(-0.2953Z^3 + 0.63508Z^2 + 4.1778Z + 0.31688),\ Z = \frac{1000}{T} - 1$$

$$K_{CH_4} = 0.1791 \exp\left[\frac{38280}{R}\left(\frac{1}{T} - \frac{1}{823}\right)\right] bar^{-1}$$

$$K_{H_2O} = 0.4152 \exp\left[-\frac{88680}{R}\left(\frac{1}{T} - \frac{1}{823}\right)\right]$$

$$K_{H_2} = 0.0296 \exp\left[\frac{82900}{R}\left(\frac{1}{T} - \frac{1}{648}\right)\right] bar^{-1}$$

$$K_{CO} = 40.91 \exp\left[\frac{70650}{R}\left(\frac{1}{T} - \frac{1}{648}\right)\right] bar^{-1}$$

reactions are favored at high temperature and low pressure, but the water-gas shift reaction is largely unaffected by the change in pressure. The six-step one-bed sorption-enhanced reaction process can obtain high purity hydrogen at low reforming temperature range of 400–650°C, which matches the operating temperature of MCFC. Therefore, the hydrogen product produced by SE-SMR may be fed directly to MCFC and reduce the consumption of energy.

THEORETICAL MODEL

A nonisothermal and nonisobaric operation is usually used for the mathematic model of the sorption-enhanced steam-methane reforming process. A model of a one-dimension, tube-packed-bed adsorptive reactor for the SE-SMR process is established and the model assumptions adopted are summarized below (4,7,14–17):

(i) The reactions were assumed to take place on the surface of the catalyst.
(ii) Gas flow is considered as an axial-dispersed plug-flow model and mass dispersion and thermal dispersion in the axial dispersion are taken into account without regard to the radial gradients.
(iii) The gas is assumed to be an ideal gas.
(iv) Pressure distribution in the fixed-bed adsorptive reactor is evaluated by the mechanical energy equation.
(v) The process is non-isothermal. The tube wall and the feed stream are maintained at the same constant temperature. The gas-phase and the catalyst/adsorbent particle are considered to be in local thermal equilibrium at all times.
(vi) The Langmuir model is used to describe the adsorption equilibrium for component CO_2 and the linear deriving-force (LDF) model is used to represent the mass transport of CO_2 to the adsorbent.
(vii) Pressure is assumed to be a linear change when pressurization or depressurization is operating.

Here is the linear deriving-force (LDF) model:

$$\frac{\partial q_{CO_2}}{\partial t} = k_{_{CO_2}}(q^*_{CO_2} - q_{CO_2}) \tag{16}$$

where k_{CO_2} is LDF mass-transfer coefficient and q_{CO_2} is the equilibrium solid-phase concentration (16).

Table 2. Model parameters for carbon dioxide adsorption kinetics (16)

$m_{CO_2}=0.65 mol/kg, b_{CO_2}=2.36\times10^{-4}\exp\left[\frac{17000}{R}\left(\frac{1}{T}-\frac{1}{673}\right)\right] Pa^{-1}(wet\ condition)$
$m_{CO_2}=0.63 mol/kg,$
$b_{CO_2}=1.69\times10^{-4}\exp\left[\frac{17000}{R}\left(\frac{1}{T}-\frac{1}{673}\right)\right] Pa^{-1}(dry\ condition)$
$k_{CO_2}=\frac{4k_mD_p}{d_p^2}\ \frac{\varepsilon_p}{\varepsilon_p+(1-\varepsilon_p)\rho_pRT(\partial q^*_{CO_2}/\partial P_{CO_2})}$

q^* is calculated by the Langmuir isotherm adsorption model:

$$q^*_{CO_2}=\frac{m_{CO_2}b_{CO_2}P_{CO_2}}{1+b_{CO_2}P_{CO_2}} \tag{17}$$

where m and b are Langmuir model constant, m, b, and k are described by Table 2.

Figure 3 shows the fixed-bed tube reactor with length L, the inside-diameter D_r, and the axial coordinate z. For the modeling, the reactor is divided into N equal elements, and the length of each part is Δz. The reactor contains a uniform mixture of the catalyst and the adsorbent with particle-size dp, and its outside wall is kept at a constant temperature.

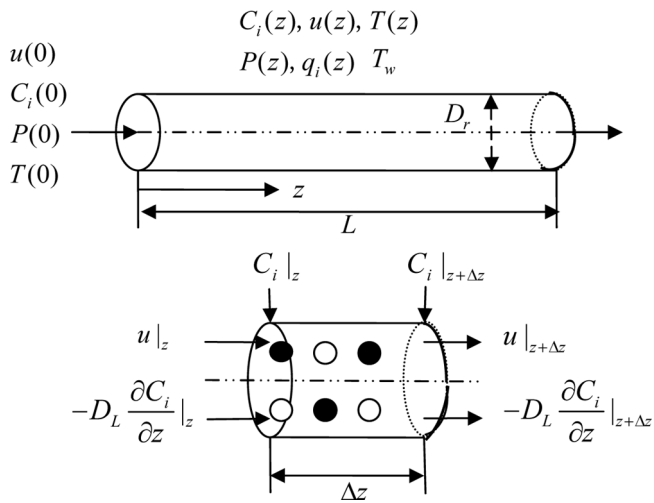

Figure 3. Configuration of fixed-bed reactor model.

From the previous assumptions, governing equations for the six steps are utilized. Thus, the overall mass balance equation is:

$$\varepsilon_t \frac{\partial C}{\partial t} + \frac{\partial (uC)}{\partial z} + \rho_{ad} \frac{\partial q_{CO_2}}{\partial t} - \rho_{cat} \sum_{j=1}^{3} \eta_j R_j = 0 \quad (i = CH_4,\ H_2O,\ H_2,\ CO,\ CO_2,\ N_2;\ j = 1, 2, 3) \tag{18}$$

Component i mass balance can be written as:

$$\varepsilon_t \frac{\partial C_i}{\partial t} + \frac{\partial (uC_i)}{\partial z} + \rho_{ad} \frac{\partial q_i}{\partial t} - \rho_{cat} \sum_{j=1}^{3} \eta_j r_i = \frac{\partial}{\partial z}\left(D_z \frac{\partial C_i}{\partial z}\right) \quad (i = CH_4,\ H_2O,\ H_2,\ CO,\ CO_2,\ N_2;\ j = 1, 2, 3) \tag{19}$$

where $\frac{\partial q_i}{\partial t} = 0$, except for $i = CO_2$; $\partial q_{CO_2}/\partial t$ is calculated by Eq. (16).

The overall heat balance equation is:

$$\left[\varepsilon_t C C_{pg} + (\rho_{ad} + \rho_{cat}) C_{ps}\right] \frac{\partial T}{\partial t} + C C_{pg} u \frac{\partial T}{\partial z} - \rho_{ad} \sum_{i=1}^{6} \left(-\Delta H_{adi} \frac{\partial q_i}{\partial t}\right) - \frac{4U}{D_r}(T_w - T) - \rho_{cat} \sum_{j=1}^{3} \eta_j\ R_j\ \Delta H_{R_j} = \frac{\partial}{\partial z}\left(k_z \frac{\partial T}{\partial z}\right) \quad (i = CH_4,\ H_2O,\ H_2, CO,\ CO_2, N_2;\ j = 1, 2, 3) \tag{20}$$

where C is the total molar concentration in the bulk phase, ε_t is the total porosity of the packed bed, u is the superficial velocity, q_{CO_2} is the CO_2 solid-phase concentration in the adsorbent, η_j is the effectiveness factor for reaction j ($j = 1, 2, 3$), D_z is the axial diffusion coefficient, ρ_{ad} is the bulk density of the adsorbent, and ρ_{cat} is the bulk density of catalyst. C_{pg} and C_{ps} are gas-phase and solid-phase heat capacity, ΔH_{adi} is the adsorption heat for the component i, ΔH_{R_j} is the reaction heat of reaction j, U is the overall bed-wall heat-transfer coefficient, T_w is the temperature of the tube-wall, and k_z is the effectiveness heat-transfer coefficient in the axial direction (15,16).

In addition, the kinetic-energy change is neglected in the mechanical-energy balance, and the kinetic-energy balance equation is described as following (15):

$$\frac{\partial P}{\partial z} = -K_D u - K_V u|u| \tag{21}$$

where K_D and K_V are the parameters of Ergun equation.

Model parameters in balance equations are shown in Table 3. D_m is the molecule diffusion coefficient, ε_b is the bed porosity , k_z^0 is the effectiveness heat-transfer coefficient in the static state, k_g is the

Table 3. Model parameters in balance equations (18–22)

$$D_L = 0.73D_m + \frac{0.5ud_p}{1 + 9.49D_m/(ud_p)}\,\mathrm{m^2/s}$$

$$K_D = \frac{150\mu_g(1-\varepsilon_b)^2}{d_p^2\varepsilon_b^3}\,\mathrm{Ns/m^4}$$

$$K_V = \frac{1.75(1-\varepsilon_b)\rho_g}{d_p\varepsilon_b^3}\,\mathrm{Ns^2/m^5}$$

$$\frac{k_z}{k_g} = \frac{k_z^0}{k_g} + 0.75(Pr)(Re_p), \frac{k_z^0}{k_g} = \varepsilon_t + \frac{1-\varepsilon_t}{0.139\varepsilon_t - 0.0339 + 2/3(k_g/k_p)},$$

$$Pr = \frac{C_{pg}\mu}{k_g}, Re_p = \frac{\rho_g u\varepsilon_t d_p}{\mu}$$

$$\frac{UD_r}{k_g} = 2.03\ Re_p^{0.8}\exp\left(-\frac{6d_p}{D_r}\right)\left(Re_p = 20 - 7600, \frac{d_p}{D_r} = 0.05 - 0.3\right)$$

$$U = 6.15\frac{k_z^0}{D_r}(Re_p \to 0)$$

gas-phase heat-transfer coefficient, k_p is the particle heat-transfer coefficient, and μ is the viscosity coefficient of fluid.

Initial Conditions

$$\text{At } t = 0 \qquad \begin{array}{l} u = 0, q_i = 0,\ y_{\mathrm{H_2O}} = 1,\ y_i = 0,\ P_{\mathrm{H_2O}} = P_H,\ P_i = 0 \\ (i = \mathrm{CH_4},\ \mathrm{H_2O},\ \mathrm{H_2},\ \mathrm{CO},\ \mathrm{CO_2},\ \mathrm{N_2}) \end{array} \tag{22}$$

The final output parameters of concentrations, temperature, and pressure along the reactor bed at each step are the initial inputs at the next step.

General Boundary Conditions for the Six Steps

$$\left(\frac{\partial y_i}{\partial z}\right)_{z=0} = \delta_1, \left(\frac{\partial y_i}{\partial z}\right)_{z=L} = \delta_2 \tag{23}$$

$$\left.\begin{array}{l} (u)_{z=0}(\text{for steps } 1, 6) \\ \left(\frac{\partial u}{\partial z}\right)_{z=0}(\text{for steps } 2-5) \end{array}\right\} = \delta_3 \tag{24}$$

$$\left.\begin{array}{l} \left(\frac{\partial u}{\partial z}\right)_{z=1}(\text{for steps } 1, 6) \\ (u)_{z=1}(\text{for steps } 2-5) \end{array}\right\} = \delta_4 \tag{25}$$

$$\left.\begin{array}{c}(P)_{z=0}(\text{for steps } 1,2)\\ \left(\frac{\partial P}{\partial z}\right)_{z=0}(\text{for steps } 3-6)\end{array}\right\}=\delta_5 \tag{26}$$

$$\left.\begin{array}{c}\left(\frac{\partial P}{\partial z}\right)_{z=L}(\text{for steps } 1,2)\\ (P)_{z=L}(\text{for steps } 3-6)\end{array}\right\}=\delta_6 \tag{27}$$

$$\left(\frac{\partial T}{\partial z}\right)_{z=0}=\delta_7,\left(\frac{\partial T}{\partial z}\right)_{z=L}=\delta_8 \tag{28}$$

where δ expressions for the six steps are listed in Tables 4–1,2.

Simplification of Governing Equations

According to the ideal-gas law $C=P/RT$ and $z=\xi L$, Eqs. (18–21) can be written as the following:

$$\begin{aligned}\frac{\partial u}{\partial \zeta}=&\frac{u}{T}\frac{\partial T}{\partial \zeta}-\frac{u}{P}\frac{\partial P}{\partial \zeta}-\frac{\rho_{ad}RTL}{P}\frac{\partial q_{CO_2}}{\partial t}+\frac{2\rho_{cat}RTL}{P}(\eta_1R_1+\eta_2R_2)\\&-\frac{\varepsilon_t L}{P}\frac{\partial P}{\partial t}+\frac{\varepsilon_t L}{T}\frac{\partial T}{\partial t}\\&(i=CH_4,\ H_2O,\ H_2,CO,\ CO_2,\ N_2;\ j=1,2,3).\end{aligned} \tag{29}$$

Table 4–1. Definition of δ

Step	δ_1	δ_2	δ_3	δ_4
1	$-\frac{u_{10}(y_{fi}-y_i)}{D_L}$	0	u_{10}	0
2	0	0	0	0
3	0	$\frac{u_{30}(y_{fi}-y_i)}{D_L}$	0	$-u_{30}$
4	0	$\frac{u_{40}(y_{fi}-y_i)}{D_L}$	0	$-u_{40}$
5	0	$\frac{u_{50}(y_{fi}-y_i)}{D_L}$	0	$-u_{50}$
6	0	$\frac{u_{60}(y_{fi}-y_i)}{D_L}$	0	0

Table 4–2. Definition of δ

Step	δ_5	δ_6	δ_7	δ_8
1	P_H	0	$-\frac{u_{10}CC_{pg}(T_f - T)}{k_z}$	0
2	$p(t)$	0	0	0
3	0	P_L	0	$\frac{u_{30}CC_{pg}(T_f - T)}{k_z}$
4	0	P_L	0	$\frac{u_{40}CC_{pg}(T_f - T)}{k_z}$
5	0	P_L	0	$\frac{u_{50}CC_{pg}(T_f - T)}{k_z}$
6	0	$P(t)$	0	$\frac{u_{60}CC_{pg}(T_f - T)}{k_z}$

Note. all velocities u_{pg} (k = 1, 2, ... 6) are taken as positive numbers, whatever the flow direction. The index k stands for the step number and the index 0 stands for the feed side in Steps 1, 3, 4, 5, 6 and outlet for Step 2.

$$\frac{\partial y_i}{\partial t} = \frac{D_L}{\varepsilon_t L^2}\left(\frac{\partial^2 y_i}{\partial \zeta^2} + \frac{1}{P}\frac{\partial P}{\partial \zeta}\frac{\partial y_i}{\partial \zeta} - \frac{1}{T}\frac{\partial T}{\partial \zeta}\frac{\partial y_i}{\partial \zeta}\right) - \frac{1}{\varepsilon_t L}\left(u\frac{\partial y_i}{\partial \zeta} + y_i\frac{\partial u}{\partial \zeta} + \frac{uy_i}{P}\frac{\partial P}{\partial \zeta} - \frac{uy_i}{T}\frac{\partial T}{\partial \zeta}\right) - \frac{\rho_{ad}RT}{\varepsilon_t P}\frac{\partial q_i}{\partial t} + \frac{\rho_{cat}RT}{\varepsilon_t P}\sum_{j=1}^{3}\eta_j R_j - \frac{y_i}{P}\frac{\partial P}{\partial t} + \frac{y_i}{T}\frac{\partial T}{\partial t}$$
$$(i = \mathrm{CH_4},\ \mathrm{H_2O},\ \mathrm{H_2},\ \mathrm{CO},\ \mathrm{CO_2}, \mathrm{N_2}; j = 1, 2, 3) \tag{30}$$

where $\frac{\partial q_i}{\partial t} = 0$, except for $i = \mathrm{CO_2}$; $\partial q_{CO_2}/\partial t$ is calculated by Eq. (16).

$$\frac{\partial T}{\partial t} = \frac{1}{\frac{\varepsilon_t C_{vg} P}{RT} + (\rho_{ad} + \rho_{cat})C_{ps}} \times \left[\begin{array}{c} \frac{k_z}{L^2}\frac{\partial^2 T}{\partial \zeta^2} - \frac{C_{pg}Pu}{RTL}\frac{\partial T}{\partial \zeta} + \rho_{ad,k}(-\Delta H_{ad\mathrm{CO_2}})\frac{\partial \bar{q}_{\mathrm{CO_2}}}{\partial t} \\ +2\rho_{cat,k}(\eta_1 R_1 \Delta H_{R_1} + \eta_2 R_2 \Delta H_{R_2}) + \frac{4U}{D_r}\left(T_{w,k} - T\right) \end{array}\right]$$
$$(i = \mathrm{CH_4},\ \mathrm{H_2O},\ \mathrm{H_2},\ \mathrm{CO},\ \mathrm{CO_2},\ \mathrm{N_2};\ j = 1, 2, 3) \tag{31}$$

$$\frac{\partial P}{\partial \zeta} = L(-K_D u - K_V u|u|) \tag{32}$$

In addition, according to assumption (vii), the following equations are obtained:

$$\frac{\partial P}{\partial t} = \begin{cases} 0 & \text{(for step 1)} \\ -(P_H - P_L)/t_2 & \text{(for step 2)} \\ 0 & \text{(for step 3)} \\ 0 & \text{(for step 4)} \\ 0 & \text{(for step 5)} \\ (P_H - P_L)/t_4 & \text{(for step 6)} \end{cases} \tag{33}$$

For the above models, the reaction rate of the three main reactions and all component i at all collocation points are calculated by Eqs. (6–9) and Eqs. (3–5). The CO_2 absorption rate is obtained by Eqs. (16,17). The idea of orthogonal collocation is used to solve the Eqs. (23–32), which are finally discretized into a set of ordinary differential equations that are solved numerically by the Gear method (4). At last, the values of velocity, pressure distribution, the effectiveness factor, the effluent mole fraction and temperature are obtained from the ordinary differential equations.

NUMERICAL SIMULATION AND ANALYSIS

Based on the description that the final state at every step is the initial conditions at the next step, the numerical simulation for the new process is carried on in series. The aim of the present paper is to simulate SE-SMR process and analyze whether gas feeds for the cathode and anode of MCFC are satisfied respectively. Table 5 lists values of basic model parameters.

Table 5. Values of basic model parameter model parameters (15,16)

$C_{pg} = 42\text{J/mol}K$	$\Delta H_{R_3} = -41100\text{J/mol}$
$C_{ps} = 850\text{J/kg}K$	$\varepsilon_b = 0.48$
$d_p = 1 \times 10^{-3}\text{m}$	$\varepsilon_p = 0.24$
$D_m = 1.6 \times 10^{-5}\text{m}^2/\text{s}(P_H)$ *or* $D_m = 5.6 \times 10^{-5}\text{m}^2/\text{s}(P_L)$	$\varepsilon_t = 0.64$
$D_p = 1.1 \times 10^{-6}\ \text{m}^2/\text{s}$	Data from present work
$m_{\text{co}_2} = 0.65\,\text{mol/kg}$ (wet condition)	$\mu = 2.87 \times 10^{-5}\text{Pa s}$
$m_{\text{co}_2} = 0.63\,\text{mol/kg}$ (dry condition)	$\rho_{ad} = 467\,\text{kg/m}^3$
$\Delta H_{\text{adco}_2} = -17000\text{J/mol}$	$\rho_{cat} = 233\,\text{kg/m}^3$
$\Delta H_{R_1} = 206000\text{J/mol}$	$\rho_p = 1300\,\text{kg/m}^3$
$\Delta H_{R_2} = 164900\text{J/mol}$	$\eta_j = 0.8\ (j = 1, 2, 3)$

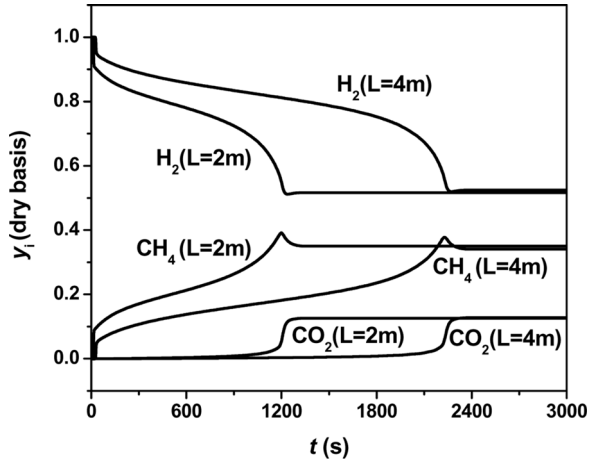

(a)

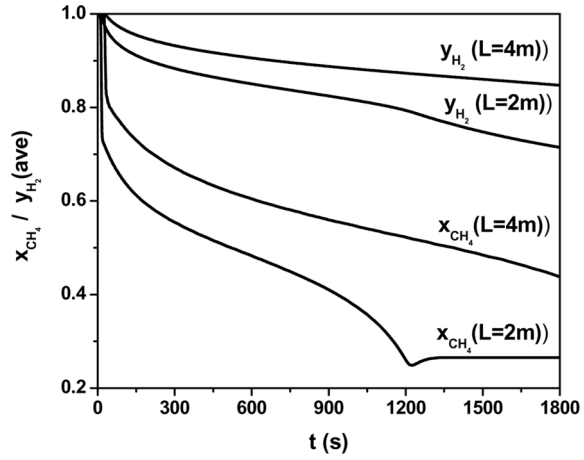

(b)

Figure 4. Reactor length effects for step 1: (a) effluent mole fractions y_i; (b) CH_4 conversion ratio X_{CH_4} and average H_2 purity y_{H2} (*ave*). Other simulation conditions see Table 6.

High-Pressure Reaction/Adsorption

Figure 4 (a) plots typical effluent mole fraction (dry basis) with reaction time (control parameters and model parameters at step 1 are listed in Table 6).

Now let us consider the situation of the reactor's length $L = 2\,\text{m}$. When $t_1 < 1230\,\text{s}$ (breakthrough point), effluent content of CO_2 is very

Table 6. Reference parameters in Step 1

$L = 2\text{m}$	$T_f = 723\text{K}$	$H_2O/CH_4 = 6$
$D_r = 2.5\text{cm}$	$T_w = 723\text{K}$	
$P_H = 445.7\,\text{kPa}$	$u_{10} = 0.08\text{m/s}$	
$D_L = 2.5483 \times 10^{-5}\,\text{m}^2/\text{s}$		$K_D = 1.0526 \times 10^4\ \text{Ns/m}^4$
$k_{co_2} = 0.1815 s^{-1}$		$K_V = 1.0981 \times 10^4\ \text{Ns}^2/\text{m}^5$
$k_z = 0.1436\text{J/m s K}$		$U = 34.8032\text{J/m}^2\ \text{K}$

low and H_2 is above 50%, due to CO_2 adsorption. Figure 4b is the CH_4 conversion ratio, and average H_2 purity (means in certain accumulation time) as a function of time. Before 1230 s, the CH_4 conversion ratio is in the range of 100% and 25%, and then the ratio is sharply reduced as the adsorbent reaches the CO_2 adsorption saturation. For a conventional reactor without the adsorbent, the temperature of the reforming reaction has to be promoted to above 600°C in order to achieve a relatively high CH_4 convention ratio. However, even at 450°C, the average hydrogen content is 80% in 1230 s in the present SE-SMR process. If the reaction time at step 1 is shortened in 600 s, the average hydrogen purity is more than 85%, and the CH_4 conversion ratio is more than 48%. So the shorter reaction time at step 1 is, the higher purity H_2 is, and vice versa. Therefore, the reaction time at step 1 was set as 1000 s in the consideration hydrogen purity and production efficiency.

The comparing results at reactor lengths of $L = 2\,\text{m}$ and $L = 4\,\text{m}$ are shown by Figs. 4 a,b. From Fig. 4a, the breakthrough time is almost proportional to the reactor length. The longer the reactor length is, which means that the more adsorbent and catalyst are filled in the reactor bed, the higher the ratio of the CH_4 conversion and the average H_2 purity are, as shown in Fig. 4b. The breakthrough time of the reactor with 4 m length is prolonged from 1230 s to 2260 s, compared to that with 2 m.

Figures 5a,b show the CO_2 gas-phase mole fraction and CO_2 solid-phase concentration at a different position of the reactor in step 1. The higher CO_2 gas-phase mole fraction is helpful for the adsorption. At the beginning of SE-SMR, CO_2 is completely adsorbed as the solid-phase concentration (CO_2 content in adsorbent) is low. With the reaction time increasing, the CO_2 gas-phase adsorption front gradually moves to the right side. For example, the CO_2 adsorption front at the 600 s is at 0.75 m and at the 1000 s moves to 1.4 m.

Figures 6a,b show the distribution of superficial velocity and temperature in the axial in step 1. As shown in Fig. 6a, at the inlet ($L = 0\,\text{m}$), the superficial velocity drops rapidly as the fast reforming reaction rate results in the temperature decreasing dramatically. Following the velocity gradually recovers and reaches a peak because of the reaction

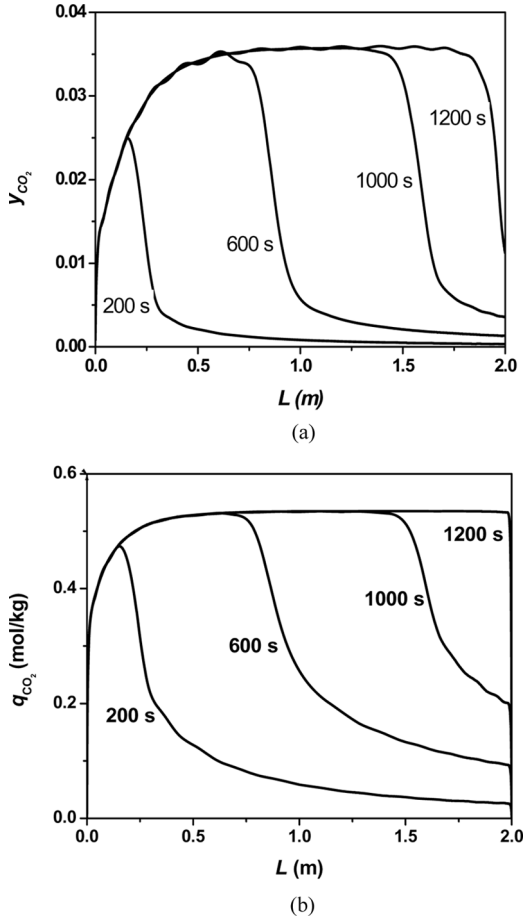

Figure 5. Distribution of CO_2 gas-phase mole fraction and CO_2 solid-phase concentration for step 1: (a) CO_2 gas-phase mole fraction y_{CO_2}; (b) CO_2 solid-phase concentration q_{CO_2}. Other simulation conditions see Table 6.

rate decreasing, the bed temperature increasing, and the gas volume inflation with reforming reactions. Then there is a velocity decrease and the velocity valley shifts to the outlet ($L = 2$ m) with time, which means CO_2 adsorption becomes a new control factor. The 600 s line is taken as an example in the following. After $L = 0.9$ m, the velocity gradually increases again as the gas volume inflation. So the alternate control factors at a different location of the bed lead to the change of velocity distribution in the reactor bed. Similarly the temperature distribution curve as the velocity distribution are shown as Fig. 6b. The temperature

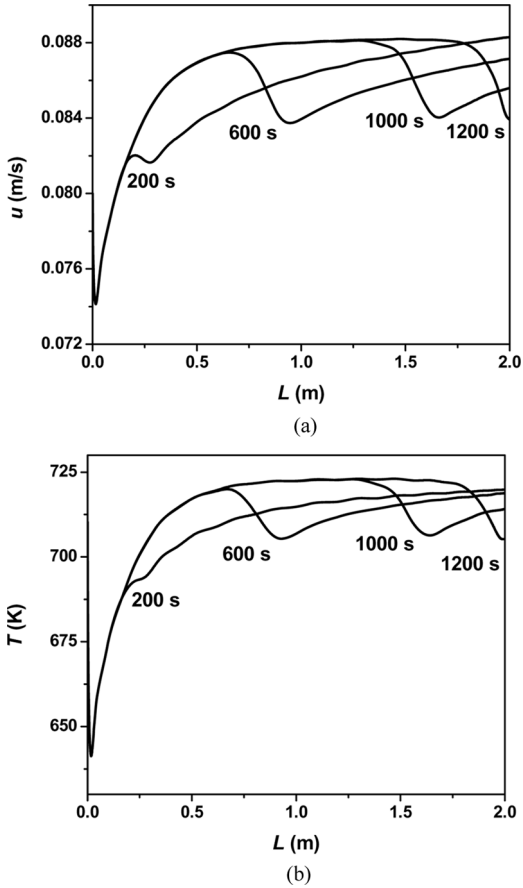

Figure 6. Distributions of superficial velocity and axial temperature for step 1: (a) superficial velocity u; (b) axial temperature T. Other simulation conditions see Table 6.

drops rapidly by ~90°C at the feed-gas entrance, and then gradually increases and near wall temperature (450°C). However, there is still a low valley at the middle as the adsorption of the CO_2 adsorbent is endothermic. The gas through the reactor bed is subjected to the flow resistance, and the calculating result shows that the pressure drops are linearly decreased along the axial from 446 kPa to 444 kPa.

The results at different superficial velocities of $u = 0.08\,\mathrm{m/s}$ and $u = 0.16\,\mathrm{m/s}$ are shown by Figs. 7a,b. From Fig. 7a, breakthrough time is decreased with the flow velocity increasing as residual time is shortened, although the rate of the reforming reactions and CO_2 adsorption

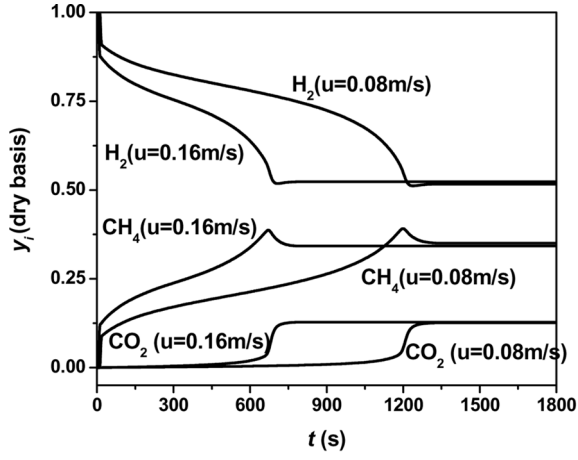

(a)

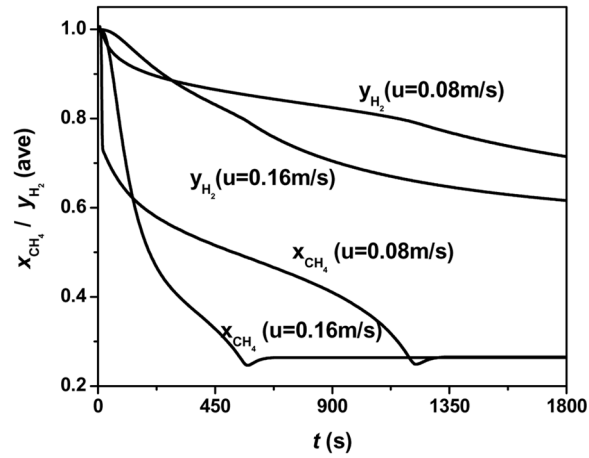

(b)

Figure 7. Superficial velocity effects for step 1: (a) effluent mole fractions *yi* (dry basis); (b) CH_4 conversion ratio X_{CH_4} and average H_2 purity y_{H_2} (*ave*). Other simulation conditions see Table 6.

are a increasing a little. It can be seen in Fig. 7b that when the flow velocity increases, the CH_4 conversion ratio and average H_2 purity decrease, on the contrary, CO_2 increases. Therefore, too high a flow velocity will result in a shorter breakthrough time.

The results at different wall temperatures of $Tw = 723\,\text{k}$, $Tw = 773\,\text{k}$ and $Tw = 823\,\text{k}$ are shown by Figs. 8a,b. As steam methane reforming reactions are strongly endothermic, the reforming process can be

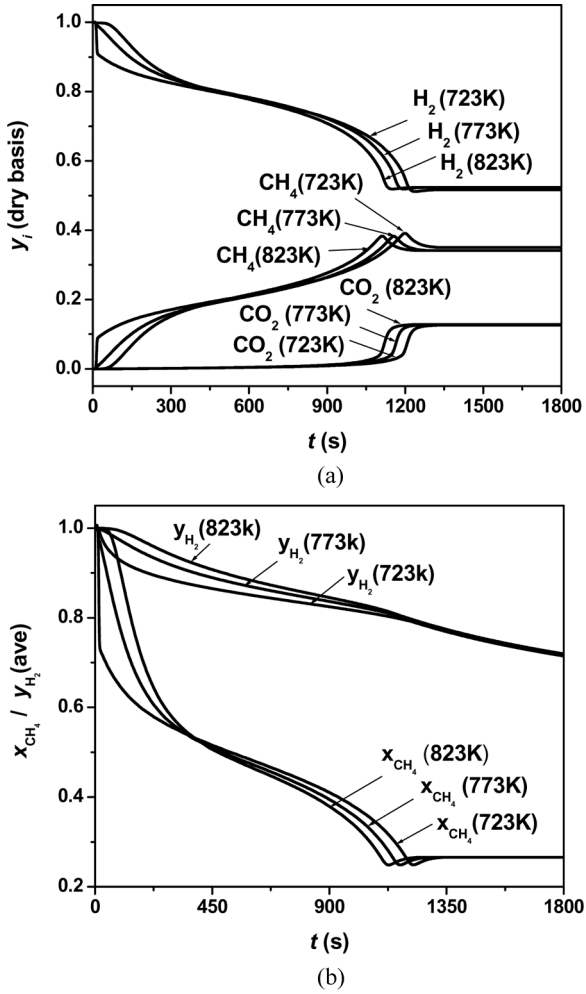

Figure 8. Wall temperature effects for step 1: (a) effluent mole fractions y_i (dry basis); (b) CH_4 conversion ratio x_{CH_4} and average H_2 purity y_{H_2} (*ave*). Other simulation conditions see Table 6.

enhanced by promoting the reaction temperature. But high temperature may weaken the CO_2 adsorption. From Fig. 8(b), the breakthrough times are 1230 s, 1170 s and 1120 s at the temperature of 723 K, 773 K, and 823 K, while the CH_4 conversion ratio and average H_2 purity increase moderately. WGS is restrained partly with temperature increasing as it is middle exothermic, and so the content of CO_2 increases slightly.

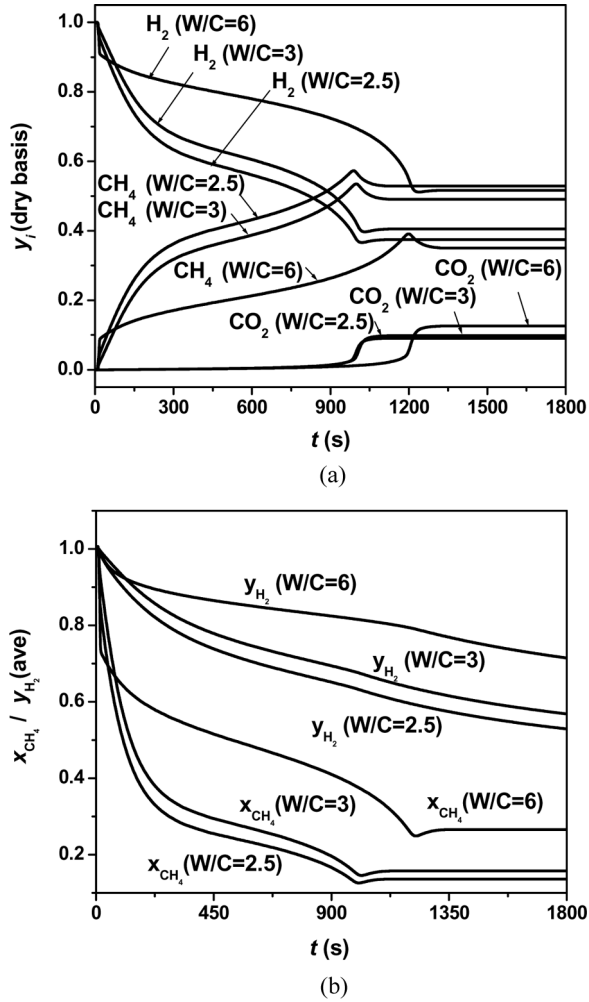

Figure 9. H_2O/CH_4 effects for Step 1: (a) effluent mole fraction y_i (dry basis); (b) CH_4 conversion ratio x_{CH_4} and average H_2 purity y_{H_2} (*ave*). Other simulation conditions see Table 6.

The effect of H_2O/CH_4 is shown by Figs. 9a,b. From the thermodynamic equilibrium, the higher H_2O/CH_4 ratio favors reforming reactions. From Fig. 9b, the CH_4 conversion ratio and the average H_2 purity increase, and the content of impurity decreases when the W/C ratio is changed from 2.5 to 6. In addition, as shown in Fig. 9a, the higher H_2O/CH_4 ratio may prolong the breakthrough time as it promotes the reforming reactions forwards, however, more energy will be consumed.

So a comprehensive consideration for H_2O/CH_4 ratio between hydrogen purity and energy consumption needs to be evaluated.

Regeneration of Spent Adsorbent and Carbon Dioxide Recycle

Conditions behind the adsorption zone are such that the adsorbent is more or less in equilibrium with the feed. Then, the equilibrium condition has to be changed for regeneration to occur. To regenerate the spent adsorbent, a low gas-phase equilibrium concentration, which is a driving force that is reversed in adsorption, is usually brought about by changing the pressure or the temperature. Here the pressure-swing regeneration (PSA) was used. Control parameters and model parameters in purge steps (step 2–6) are listed in Table 7.

Low-pressure purge with nitrogen for CO_2 desorption (steps 3 and 4) was used. In one circle, axial CO_2 distributions of the gas-phase and the solid-phase in the reactor bed are simulated. The results at the end of each step are shown in Figs. 10a,b.

In the pressure-swing adsorption, the operation pressure is changed with the adsorption taking place at high pressure and desorption at low pressure. The reactor pressure is reduced from 446 kPa to 126 kPa in 150 s. During the depressurization, CO_2 releasing and reforming reactions are continuously carried out. Its effluent is burnt. Control parameters and model parameters in step 2 are listed in Table 7.

After the depressurization, the following step is the 1st nitrogen purge to remove hydrogen in the reactor bed. There is a little amount of CO_2 releasing in this step. The modeling result shows that there is almost no H_2 in the effluent stream after 12 s. Only near at $\boldsymbol{L} = 0$, there are a little CO_2 desorbed. The purge stream is recovered as fuel.

Table 7. Control parameters and evaluated model parameters in Purge Steps

$L = 2\,\text{m}$		$t_2 = 150\,\text{s}$
$D_r = 2.5\,\text{cm}$	$u_{30} = -0.1\,\text{m/s}$	$t_3 = 50\,\text{s}$
$P_L = 125.7\,\text{kPa}$	$u_{40} = -0.3\,\text{m/s}$	$t_4 = 1800\,\text{s}$
$P_H = 445.7\,\text{kPa}$	$u_{50} = -0.1\,\text{m/s}$	$t_5 = 50\,\text{s}$
$T_w = 723\,\text{K}$	$u_{60} = -0.1\,\text{m/s}$	$t_6 = 150\,\text{s}$
$T_f = 723\,\text{K}$		

$K_D = 1.0526 \times 10^4 \text{Ns/m}^4$ $U = 34.8032\,\text{J/m}^2\text{K}$

Step 2	Steps 3,4,5	Step 6
$D_L = 1.2844 \times 10^{-5}\,\text{m}^2/\text{s}$	$D_L = 4.8798 \times 10^{-5}\,\text{m}^2/\text{s}$	$D_L = 1.2844 \times 10^{-5}\,\text{m}^2/\text{s}$
$k_{co_2} = 0.1815 s^{-1}$	$k_{co_2} = 0.1\,\text{s}^{-1}$	$k_{co_2} = 0.1\,\text{s}^{-1}$
$k_z = 0.1436\,\text{J/m s K}$	$k_z = 0.1422\,\text{J/m s K}$	$k_z = 0.1422\,\text{J/m s K}$
$K_V = 17.8126\,\text{P/TN s}^2/\text{m}^5$	$K_V = 3.0969 \times 10^3\,\text{N s}^2/\text{m}^5$	$K_V = 17.8126\,\text{P/TN s}^2/\text{m}^5$

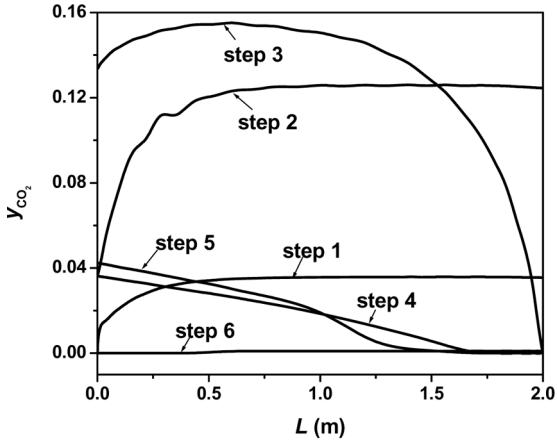

(a)

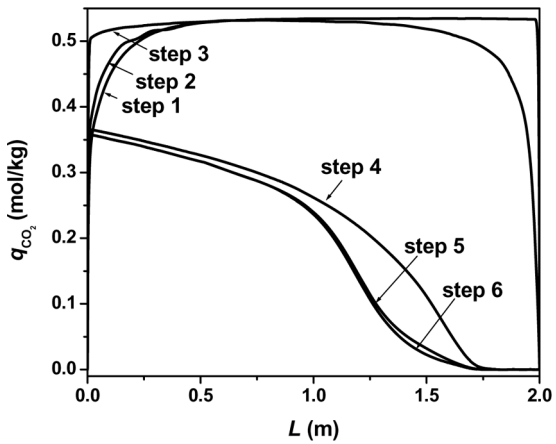

(b)

Figure 10. Distribution of CO_2 gas-phase mole fraction and CO_2 solid-phase concentration in one cycle. Other simulation conditions see Tables 6,7.

Low-pressure purge with nitrogen for CO_2 desorption (step 5) is definitely a substantial step for the whole novel system. As stated above, low-pressure nitrogen purge plays the main role in the adsorbent regeneration, and the other is for the preparation of the MCFC cathode feed. In step 5, most of the CO_2 is desorbed, but there is still a little remaining CO_2 between $\boldsymbol{L} = 0$ m and $\boldsymbol{L} = 1.2$ m of the reactor, as shown in Fig.10b. The longer the purging time is, the nearer the completeness of the CO_2

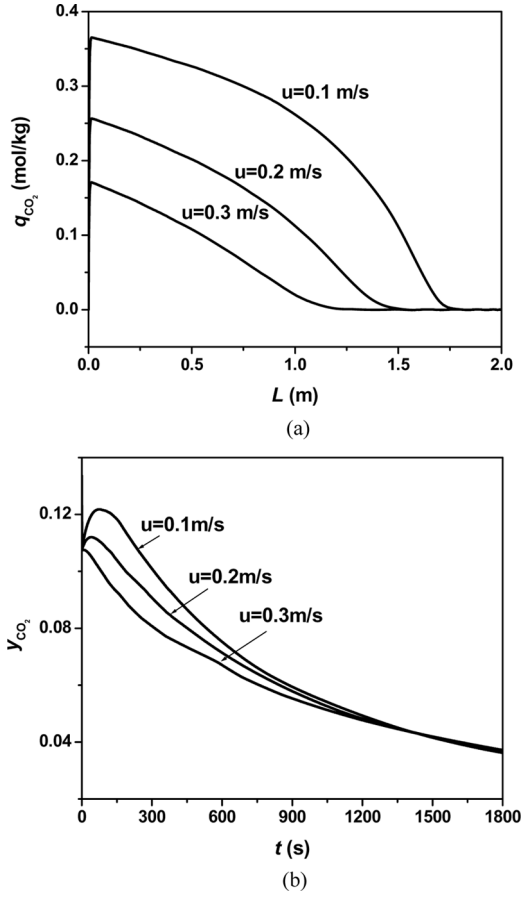

Figure 11. Effects of superficial velocity of nitrogen purge stream in step 4: (a) axial distribution of CO_2 (solid phase) (regenerative degree); (b) effects of superficial velocity of nitrogen purge stream on CO_2 mole fractions at outlet ($L = 0$). Other simulation conditions see Tables 6,7.

desorption is. On the other hand the, desorption efficiency may gradually drop with the increase of reaction time.

In addition, the desorbed CO_2 concentration decreases and the amount of CO_2 desorption increases with the nitrogen velocity increasing as shown in Figs. 11a,b. But the velocity of the nitrogen purge stream hardly can influence the largest concentration (about 14%) of the desorbed CO_2.

From Figs. 12a,b, when the regeneration temperature is changed from 723 K to 823 K, the axial distribution concentration of the CO_2 gas phase and the final amount of CO_2 desorption slightly increase.

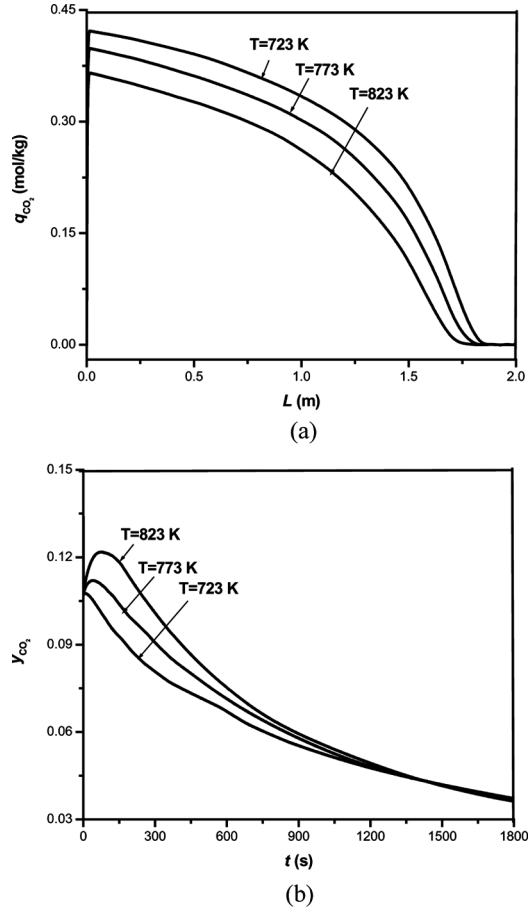

Figure 12. Effects of regeneration temperature in step 4: (a) axial distribution of CO_2 (solid phase) (regenerative degree); (b) CO_2 mole fractions at outlet ($L = 0$). Other simulation conditions see Table 6,7.

Low-pressure purge with reformed gas for the CO_2 desorption is carried out after the regeneration. The reformed gas is countercurrently input at 126 kPa in order to remove N_2 in the reactor bed and further desorbs the CO_2 in the adsorbent.

In the pressurization step, the high pressure stream of reformed gas produced is used to pressurize to 446 kPa. From Figs. 10a,b, a little CO_2 adsorbed in the adsorbent is dissolved and the CO_2 concentration in the solid phase decreases slightly, as increasing pressure always favors the CO_2 adsorption. The control parameters and the evaluated model parameters in the pressurization are shown in Table 7. After this step,

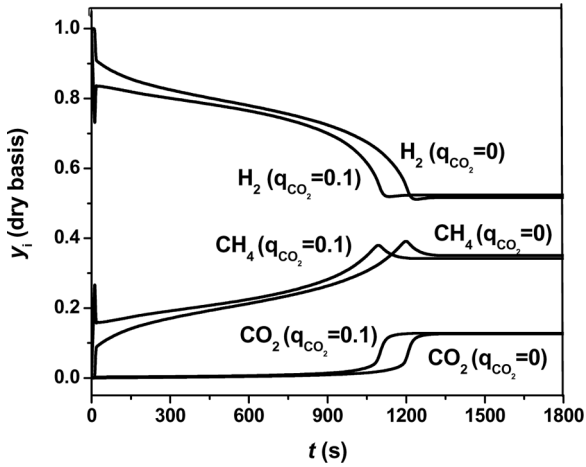

Figure 13. Effects of solid phase (regeneration degree) on gas compositions at outlet ($L = 2$ m). Other simulation conditions see Table 6.

the regeneration of the adsorbent in the fixed-bed reactor is completed and the remaining CO_2 concentration (solid phase) drops to an acceptable level for the next cycle.

CO_2 Concentration (Solid Phase) in the Adsorbent

In the above calculation, it is assumed that the CO_2 adsorbent is fresh, i.e., $q_{CO2} = 0$, at the initial state of the high-pressure adsorption-enhanced reaction. However, desorption of CO_2 from the adsorbent is not complete and uniform in a real case. The remaining CO_2 concentration (solid phase) is variable with the position of the reactor bed. For the convenience in this section, it is assumed that the CO_2 concentration (solid phase) in the adsorbent regenerated is uniform. The regeneration degree of the adsorbent has great effect on the hydrogen production, as shown in Fig. 13. The breakthrough time of high-pressure, adsorption-enhanced reaction is curtailed to 1120 s for $q_{CO2} = 0.1$ mol/kg. CO_2 desorption may be improved by enhancing the regeneration, such as prolonging the time of the air purge or the superficial velocity of the purge stream. But too highly complete regeneration will result in a longer purge time or more energy consumption.

System Analysis

A typical arrangement of a pressure-swing unit consists of at least two parallel reactors (10), one adsorbing and the other regenerating, to run

the cycle in a continuous mode. In the present process, the adsorbent regeneration time is twice that of the sorption-enhanced reaction time. Hence, more than two reactors are needed for continuous H_2 supply. For simplicity, we consider a three-reactor configuration for the continuous supply of the H_2 stream and regeneration.

Here the sorption-enhanced reaction time is set as 1000 s, and the regeneration time $t_2 + t_3 + t_4 + t_5 + t_6 = 175\,\text{s} + 150\,\text{s} + 1400 + 150\,\text{s} + 125\,\text{s} = 2000\,\text{s}$. Therefore, the three reactors are arranged, in which one reactor undergoes reactions to produce the H_2 stream, while the other two reactors are at the regeneration step.

The reformed gas product as the anode feed comes from step 1 (high-pressure reaction/adsorption). From the results of the numerical simulation in step 1, in the period of 1000 s, hydrogen production is 0.85 mol/1000 s for each tube (according to the simulation result) and the average H_2 purity is above 81%. Hufton et al. (2000) pointed out that 50–90% H_2 purity is acceptable in fuel cell applications, so the reformed gas meets the MCFC's need, which can be directly input as its temperature is near the operating temperature of MCFC.

In contrast to the other fuel cells, the MCFC requires a supply of CO_2 to the cathode and meanwhile, CO_2 is formed at the anode. The theoretical mole ratio of CO_2/air in the cathode reaction in MCFC is 28.57%. It is usual practice that a part of the anode exit gases, after complete combustion, is introduced into the cathode inlet gas stream.

In the present process, a carbon dioxide recycle mechanism is suggested for the cathode feed of MCFC from flue gas by burning with excess air to achieve a proper CO_2/air ratio (about 30: 70). It is easy to control the CO_2/air ratio and get high energy efficiency.

CONCLUSIONS

A novel system is presented and analyzed based on the combination of a six-step SE-SMR process and MCFC, and some useful conclusions are obtained according to the results of the numerical simulation:

(i) A fuel cell grade hydrogen product (above 80%) in the reaction/adsorption time of 1000 s for each circle time of 1400 s can be obtained at a lower temperature (450°C) compared with the conventional steam-reforming process;
(ii) In the SE-SMR process, both the process stream and the purge stream are target products, which are used as anode feed and cathode feed in MCFC, respectively;

(iii) A carbon dioxide recycle mechanism is suggested for cathode feed of MCFC from flue gas by over air burning to achieve a proper CO_2/air ratio (about 30:70), which is a little different from the normal MCFC system;
(iv) The similar operating temperatures of SE-SMR and MCFC mean that the hydrogen produced can be directly introduced into the MCFC as fuel.

Therefore, the novel electricity generation system, which can operate with the lower energy consumption and high purity hydrogen feed, is helpful for the MCFC'S life time and performance.

Nevertheless, there is still much work to do, including:

(i) There is a strong demand that high capacity adsorbent for carbon dioxide that is suitable for large-scale industrial application;
(ii) The SE-SMR reactor needs special design and a optimization for scale of the novel electricity generation system should be done.

NOTATION

b_{CO_2}	Langmuir model constant for component CO_2 [Pa^{-1}]
C	total molar concentration in the bulk phase [mol/m^3]
C_i	molar concentration of gas-phase component*i* [mol/m^3]
C_{pg}	gas-phase heat capacity [$J/mol \cdot K$]
C_{ps}	solid-phase heat capacity [$J/kg \cdot K$]
d_p	particle diameter [m]
D_m	molecular diffusivity [m^2/s]
D_p	combination of molecular and Knudsen diffusivity [m^2/s]
D_L	axial dispersion coefficient [m^2/s]
D_r	reactor diameter [m]
k_{CO_2}	LDF mass-transfer coefficient [s^{-1}]
k_g	gas-phase thermal conductivity [$J/m \cdot s \cdot K$]
k_j	rate constant of reaction *j*, $j = 1,2$ [$molPa^{0.5}/kg(cat)$] $j = 3$ [$mol//kg(cat)s$]
k_p	particle thermal conductivity [J/msK]
k_z	effective thermal conductivity [J/msK]
K_D	Ergun equation coefficient [N/sm^4]
K_j	equilibrium constant of reaction *j* $j = 1,2$ [Pa^2]
K_V	Ergun equation coefficient [Ns^2/m^5]
L	reactor length [m]
m	Langmuir model constant [mol/kg]

P	local total pressure [Pa]
P_i	partial pressure of gas-phase component i [Pa]
P_H	high pressure [Pa]
P_L	low pressure [Pa]
q_i	solid-phase concentration for component i [mol/kg] (ad)
q^*	equilibrium solid-phase concentration [mol/kg]
r_i	consumption rate of component i [mol/kg(cat)s]
R_j	reaction rate of component i [mol/kg(cat)s]
R	universal gas constant [J/mol.K]
S	cross-sectional area [m^2]
t	time [s]
ti	operational time for step i [s]
T	temperature [K]
T_f	feed gas temperature [K]
T_w	wall temperature [K]
u	superficial velocity [m/s]
u_{i0}	initial superficial velocity for step i [m/s]
U	overall bed-wall heat-transfer coefficient [J/m^2K]
y_{fi}	gas-phase mole fraction of component i in the feed
y_i	gas-phase mole fraction of component i
z	axial coordinate in bed [m]

Greek Letters

ε_b	bed porosity
ε_p	adsorbent porosity
ε_t	total bed porosity
η_j	catalyst effectiveness factor
ξ	z/L
μ	viscosity of fluid [kg/m.s]
ρ_{ad}	bulk density of adsorbent [kg/m^3]
ρ_{cat}	bulk density of catalyst [kg/m^3]
ρ_g	gas-phase density [kg/m^3]
ρ_p	adsorbent pellet density [kg/m^3]
$-\Delta H_{\text{adi}}$	adsorption heat of component i [J/mol]
ΔH_{R_j}	reaction heat of reaction i [J/mol]

ACKNOWLEDGEMENT

This work was supported by National Natural Science Foundation of China (no. 20576071).

REFERENCES

1. Brouwer, J.; Jabbari, F.; Leal, E.M.; Orr, T. (2006) Analysis of a molten carbonate fuel cell: Numerical modeling and experimental validation. *Journal of Power Sources*, *158* (1): 213.
2. Iaquaniello, G.; Mangiapane, A. (2006) Integration of biomass gasification with MCFC. *International Journal of Hydrogen Energy*, *31* (3): 399.
3. Tomczyk, P. (2006) MCFC versus other fuel cells—Characteristics, technologies and prospects. *Journal of Power Sources*, *160* (2): 858.
4. Xiu, G.H.; Li, P.; Rodrigues, A.E. (2002) Sorption-enhanced reaction process with reactive regeneration. *Chemical Engineering Science*, *57* (18): 3893.
5. Xiu, G.H.; Li, P.; Rodrigues, A.E. (2003) New generalized strategy for improving sorption-enhanced reaction process. *Chemical Engineering Science*, *58* (15): 3425.
6. Reijers, H.T.J.; Valster-Schiermeier, S.E.A.; Cobden, P.D.; Van der Brink, R.W. (2006) Hydrotalicte as CO_2 sorbent for sorption-enhanced steam reforming of methane. *Industrial Engineering Chemical Research*, *45*: 2522.
7. Yong, Z.; Mata, V.; Rodrigues, A.E. (2001) Adsorption of carbon dioxide onto hydrotalcite-like compounds (HTlcs) at high temperatures. *Industrial Engineering Chemical Research*, *40* (1): 204.
8. Hufton, J.R.; Waldron, W.; Weigel, S.; Rao, M.; Sircar, S. (2000) Sorption enhanced reaction process (SERP) for the production of hydrogen. *Proceedings of U.S. DOE Hydrogen Program Review*, *1* (1): 70.
9. Xiu, G.H.; Soares, J.L.; Li, P.; Rodrigues, A.E. (2002) Pressure swing adsorptive reactors: Simulation of five-step one-bed sorption-enhanced reaction process. *American Institute of Chemical Engineering Journal*, *48* (12): 2817.
10. Carvill, B.T.; Hufton, J.R.; Anand, M.; Sircar, S. (1996) Sorption-enhanced reaction process. *American Institute of Chemical Engineering Journal*, *42* (10): 2765.
11. Iordanidias, A.A.; Kechagiopoulos, P.N.; Voutetakis, S.S.; Lemonidou, A.A.; Vasalos, I.A. (2006) Autothermal sorption-enhanced steam reforming of bio-oil/biogas mixture and energy generation by fuel cells: Concept analysis and process simulation. *International Journal of Hydrogen Energy*, *31* (8): 1058.
12. Lysikova, A.I.; Trukhan, S.N.; Okunev, A.G. (2008) Sorption enhanced hydrocarbons reforming for fuel cell powered generators. *International Journal of Hydrogen Energy*, *33* (12): 3061.
13. Xu, J.; Froment, G.F. (1989). Methane steam reforming, methanation and water gas shift: I. Intrinsic kinetics. *American Institute of Chemical Engineering Journal*, *35*: 96.
14. Silva, J.A.C.; Rodrigues, A.E. (1998) Separation of n/iso-paraffins mixtures by pressure swing adsorption. *Separation Purification and Technology*, *13* (3): 195.
15. Ding, Y.; Alpay, E. (2000) Adsorption-ehanced steam-methane reforming. *Chemical Engineering Science*, *55* (18): 3929.

16. Ding, Y.; Alpay, E. (2000) Equilibria and kinetics of high temperature CO_2 adsorption on hydrotalcite adsorbent. *Chemical Engineering Science*, *55* (17): 3461.
17. Sereno, C.; Rodrigues, A.E. (1993) Can steady-State momentum equations be used in modeling pressurization of adsorption beds. *Gas Separation and Purification*, *7*: 167.
18. Edwards, M.F.; Richardson, J.F. (1968) Gas dispersion in packed beds. *Chemical Engineering Science*, *23*: 109.
19. Ergun, S. (1952) Fluid Pow through packed columns. *Chemical Engineering Progress*, *48*: 89.
20. Malek, A.; Farooq, S. (1997) Study of a six-bed pressure swing adsorption process. *American Institute of Chemical Engineering Journal*, *43*: 2509.
21. Li, C.H.; Finlayson, B.A. (1977) Heat transfer in packed bed-a reevaluation. *Chemical Engineering Science*, *32*: 1055.
22. De Wash, A.P.; Froment, G.F. (1972) Heat transfer in packed bed. *Chemical Engineering Science*, *27*: 567.